

Fast rotation of nuclei with extreme isospin in the vicinity of neutron and proton drip lines.

A. V. Afanasjev¹, S. Teeti¹ and A. Taninah²

¹Department of Physics and Astronomy, Mississippi State University, Starkville, MS 39762, USA

²Department of Chemistry and Physics, Louisiana State University, Shreveport, Louisiana 71115, USA

E-mail: aa242@msstate.edu

Abstract. The analysis of the present understanding of collective rotation in very neutron-rich nuclei is presented. It is shown that collective rotation can lead to the increase of stability of rotational states with increasing spin. The detailed investigation of rotational excitations in very proton-rich nuclei confirms this conclusion and indicate that experimental studies of such features are more feasible in the nuclei near proton drip line. They also show that rotational bands which are proton quasi-bound at zero or low spins can be transformed into proton bound ones at high spin by collective rotation of nuclear systems. This is due to strong Coriolis interaction which acts on high- j or strongly mixed M orbitals and drives the highest in energy occupied single-particle states into negative energy domain. These physical mechanisms lead to a substantial extension of the nuclear landscape beyond the spin zero proton drip line. In addition, a new phenomenon of the formation of giant proton halos in rotating nuclei emerges: it is triggered by the occupation of strongly mixed M intruder orbitals.

Keywords: extremely neutron- and proton-rich nuclei, high spin, covariant density functional theory

1. Introduction

The rotation is one of the most important collective excitations in atomic nuclei. It leads to a lot of interesting physical phenomena such as multiply rotational bands in a specific nucleus based on different particle-hole excitations [1, 2, 3], superdeformation [4, 5, 6], gradual evolution of collectivity in rotational bands up to their final termination in a single-particle terminating states [7], magnetic and anti-magnetic rotational bands [8, 9], clusterization [10, 11, 12] etc. However, with a few exceptions experimental and theoretical studies of rotational excitations have been carried out for nuclei located not far away from the β -stability valley and more frequently on its proton-rich side in the direction of proton-drip line. On the other hand, the introduction of new experimental facilities such as FRIB will potentially extend the studies of rotational structures to significantly more proton- and neutron-rich nuclei as compared with those investigated till now.

In the nuclei experimentally investigated so far the rotational excitations reveal themselves via the rotational bands the rotational states of which are connected by γ -transitions of different multipolarity i.e. by the E2 transitions in the rotational bands which have an electric character and by the M1 transitions in magnetic bands [3, 7, 8, 9]. The rotational states are discrete because all occupied single-particle states in the nucleonic configurations of the bands are particle bound: typical γ -decay time τ_γ is of the order of 10^{-9} s.

The situation is expected to be different in the nuclei located near the drip lines since the last occupied single-particle state(s) of nucleonic configuration can be located at positive energies. This will lead to an opening of other channels of the decay such as proton and neutron emission competing with the γ -decay from rotational states. However, only few papers have been dedicated to theoretical studies of rotational motion in the nuclei near neutron drip line [13, 14, 15, 16] and no experimental studies for such systems exist. The situation is opposite for the nuclei near the proton drip line: the rotational bands based on ground state proton-emitting configurations have been experimentally observed in the ^{59}Cu [17] and ^{141}Ho [18] nuclei but theoretical studies of rotational motion in the nuclei located near proton drip line have not been carried out. Thus, the goals of the present paper are the following: (i) to review existing theoretical studies and to extract the general features of rotational motion in the nuclei located near the drip lines and (2) to carry out a detailed investigation of rotational structures in the nuclei located near the proton drip line.

The paper is organized as follows. An overview of theoretical studies of rotational structures in the nuclei near neutron drip line is presented in Sec. 2. Open questions related to rotational motion in the nuclei located near the drip lines and their resolution are discussed in Sec. 3. The general features of the rotation in proton-rich nuclei and the differences with the situation near the neutron-drip line are briefly overviewed in Sec. 4. The details of theoretical calculations are presented in Sec. 5.1. The birth of proton-bound rotational bands is illustrated in Sec. 6 on the example of the ^{14}Ne and

^{67}Kr nuclei. The emergence of giant proton halos at very high spin is discussed in Sec. 7. Rotating induced extension of the nuclear landscape is considered in Sec. 8. Finally, Sec. 9 summarizes the results of our paper.

2. Rotation in neutron-rich nuclei near neutron-drip line: the current status

At present, there are no experimental studies of rotational bands in the neutron-rich nuclei located at or near neutron drip line. However, several theoretical studies reveal interesting features of rotational excitations in such nuclei which are distinctly different from those seen in known nuclei. They emerge from the possibility of neutron emission. Note that nucleonic configuration is a system of nucleons distributed over specific set of single-particle states which is bound together for a time τ_{conf} which is substantially larger than characteristic nuclear timescale of 10^{-22}s (see Ref. [19]). Note that setting up collective rotation also requires time which is substantially larger than above mentioned timescale. Thus, the rotational states cannot be built on the occupation of the single-particle states which belong to the scattering continuum (i.e. from the states with orbital momentum $l \neq 0$ located at the energies larger than E_B (see Fig. 1(a) and Ref. [19]) or from positive energy single-particle states with $l = 0$ (see Refs. [14, 15]).

Nucleonic configurations in very neutron-rich nuclei which lead to rotational states are built from the combination of bound $|B\rangle$ and quasi-bound $|QB\rangle$ states (see Fig. 1(a)) and the properties of occupied $|QB\rangle$ state(s) define the stability of configuration with respect of neutron emission. Note that the lifetimes for neutron emission from the ground and low-spin states in the $A \leq 28$ nuclei located near neutron-drip line, for which experimental data exist, are very short: due to low value of centrifugal barrier the largest half life is only by two orders of magnitude larger than 10^{-22} s [20]. Even in this kind of situation, it is possible in very neutron-rich ^{11}Be and ^{39}Mg nuclei to build rotational bands formed on the basis of the nucleonic configurations in which the occupied $|QB\rangle$ state has orbital momentum $l \neq 0$ [14, 15]. The rotational states of such bands have a width because of coupling with continuum [14, 15] and their observation is possible only via neutron emission which proceeds substantially faster than the typical γ -decay.

The rotational bands calculated in these two very neutron-rich nuclei have two interesting features. First, the states of favored in energy signature branch of the ground state $1/2^+$ rotational band in ^{11}Be are predicted to have small neutron decay width of around 200 keV, while these widths are substantially larger (around 0.7 MeV) for the states in unfavored in energy signature branch [14]. This means that unfavored signature states are more unbound (i.e. located at higher energy and thus facing lower effective barrier with smaller width) than favored ones. The same features exist in our cranked relativistic mean field (CRMF) calculations: the ground state rotational band in ^{11}Be is based on the deformed $1/2[220]$ Nilsson state emerging from the $d_{5/2}$ spherical neutron subshell and there is sufficient signature splitting between favored and unfavored signature branches to account for the difference in decay width. Second, the

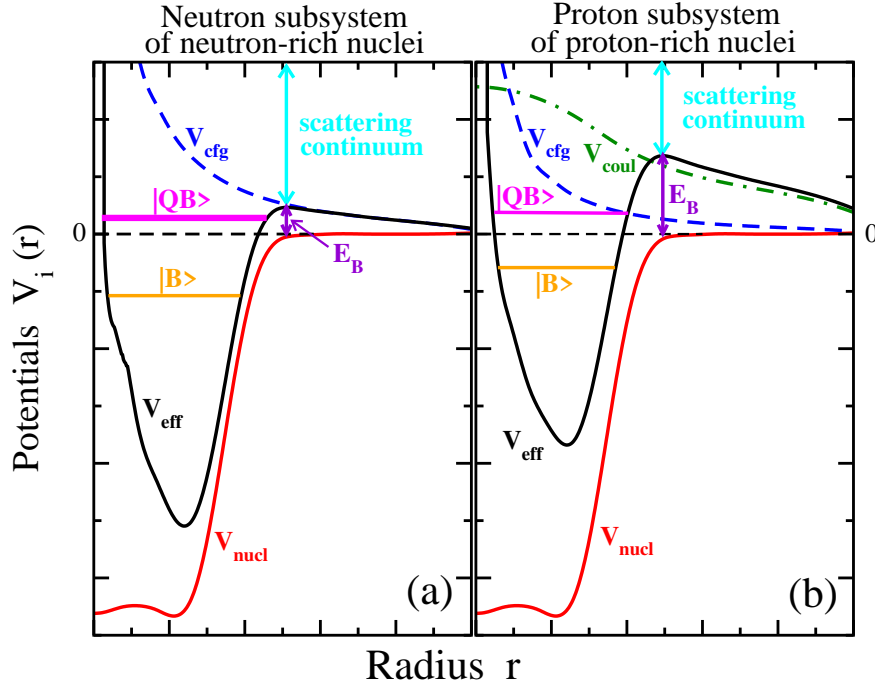


Figure 1. A schematic representation of nuclear bound, quasi-bound (resonant) and scattering states. Here, $V_{eff}(r) = V_{nucl} + V_{cfg} + V_{Coul}$ represents effective potential formed by nucleonic (central) V_{nucl} , centrifugal V_{cfg} and Coulomb V_{Coul} potentials. Note that the Coulomb potential is absent in the neutron subsystem. E_B is the height of the barrier of the effective potential the peak of which is located in near-surface region of the nucleus. Decaying quasi-bound states are located at the energies e_i in the range of $0 < e_i < E_B$. See text for further details.

calculations of Ref. [15] for rotational band in ^{39}Mg based on deformed $1/2[321]$ Nilsson state show drastic decrease of the decay width with increasing angular momentum in the band from very broad to very narrow resonances. This is due to the fact that the structure of odd neutron in low and middle spin $1/2^-$, $3/2^-$, $5/2^-$, $7/2^-$ rotational states contains substantial contribution from the $l = 1$ $p_{3/2}$ spherical subshell while the one for high-spin $9/2^-$ and $11/2^-$ states is dominated by the $l = 3$ $f_{7/2}$ states. As a consequence, the drastic reduction of the decay width at high spin is due to the substantial increase of centrifugal barrier.

Note that the calculations of rotational structures in Refs. [14, 15] have been carried within the particle-plus-core model based on a nonadiabatic coupled-channel formalism and the Berggren single-particle ensemble. The advantage of this model is that it takes explicitly into account bound states, narrow resonances, and the scattering continuum. However, it uses the core fitted to existing low spin data in neighboring even-even nucleus and assumes fixed deformation for the single-particle Woods-Saxon potential which does not depend on angular momentum of rotational states. However, the deformation of rotational states (especially in light nuclei) is expected to change (drastically) with increasing angular momentum (see, for example, Refs. [3, 7, 21, 22] and references quoted therein).

This deficiency of the particle-plus-core model can be taken care in the cranking model which defines the deformation of a rotational state of interest in a fully self-consistent way. However, before our investigations there was only one exploratory study of weakly-bound neutron-rich even-even $^{30-38}\text{Ne}$ and $^{32-40}\text{Mg}$ nuclei within the cranked Skyrme-Hartree-Fock (CSHF) approach without pairing in Ref. [13]. The deformed configurations considered in this paper have the valence neutrons in weakly-bound $f_{7/2}$ high- j intruder states, located at small negative energies. They have large centrifugal barrier due to large orbital angular momentum $l = 3$ which leads to a good localization of their wavefunctions (see Ref. [13]).

3. Open questions and their resolution

However, there are additional factors at play not considered in these studies. For example, they examine only low spin yrast or near yrast configurations with relatively modest deformation. However, the angular momentum which can be built within such rotational bands is quite limited. Let us take as an example the ^{38}Ne nucleus. The lowest configuration in this nucleus has the $\pi(d_{5/2})_4^2 \otimes \nu(\text{core})_0$ structure with respect of the ($Z = 8, N = 28$) core with maximum angular momentum $I_{max} = 4^+$ and the deformed configuration built by two particle - two hole excitation across the $N = 28$ spherical shell gap has the structure $\pi(d_{5/2})_4^2 \otimes \nu(f_{7/2})_6^{-2}(f_{5/2})_4^2$ with maximum angular momentum $I_{max} = 14^+$. Note that the configurations are labelled here in the language of Ref. [7]. Other examples of limited angular momentum in the rotational structures built on the ground or excited configurations of light nuclei of interest are discussed in Sec. 12.4 of Ref. [3] (for example, ground state rotational band of ^{20}Ne terminates at $I_{max} = 8^+$), Sec. 7 of Ref. [7] and Sec. III of Ref. [22]. Thus, this analysis leads to a *first question*, namely, "What is the mechanism of the creation of higher angular momentum in the nuclei of interest and whether such mechanism leads to a destruction or stabilization of rotational motion in a given nucleonic configuration?"

Absolute majority of rotational bands studied so far both in experiment and in theory are built on nucleonic configurations which are particle bound, i.e. all occupied single-particle states of these configurations are located at negative energies. Thus, appropriate name for this class of rotational bands is *particle-bound rotational bands*. The second class of rotational bands, in which at least one occupied single-particle state of respective nucleonic configuration is located at positive energy below E_B (i.e. the state is quasi-bound [23, 24, 25]‡), has been suggested in Refs. [14, 15]. There is no well established name for this class of bands: they were called as rotational bands embedded in the continuum in Ref. [15] and as resonance bands in Ref. [16]. In the present paper we call them as *quasi-bound rotational bands* to stress that their states are bound for sufficiently long time to form a collective structure and that they can decay by particle emission. This discussion raises the *second and third questions*, namely, "Can these two

‡ Quasi-bound states are denoted also as quasistationary or resonance states in the literature (see, for example, Ref. [25]).

classes of rotational bands coexist in the same nucleus?" and "Whether the transition from one class of collective rotation to another is possible within a rotational band built on a fixed nucleonic configuration?".

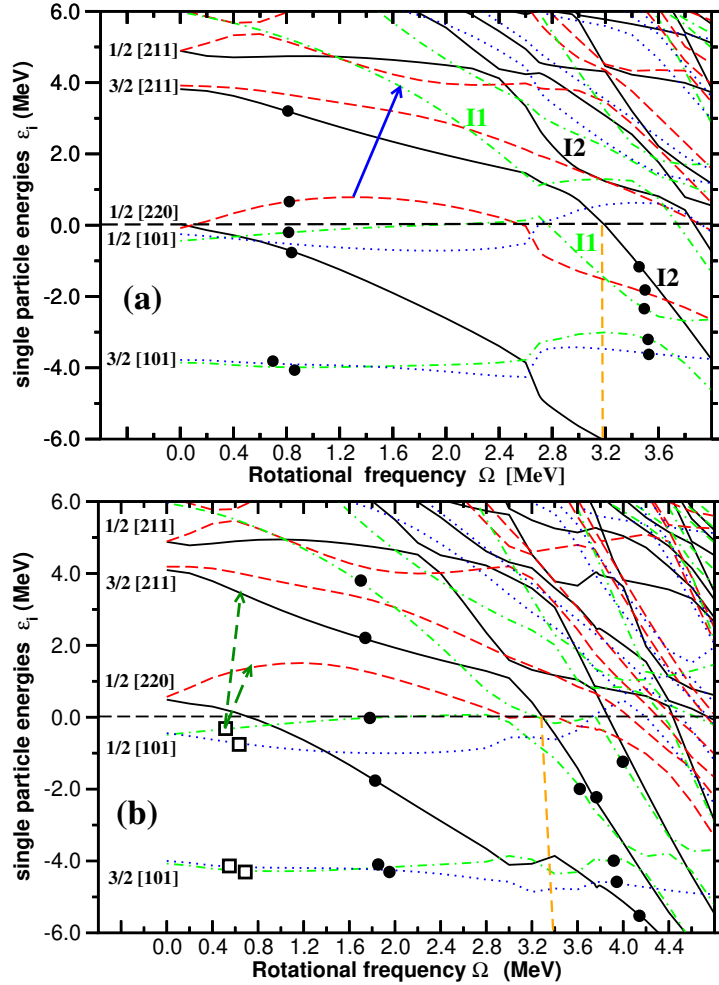


Figure 2. Proton single-particle energies (routhians) in the self-consistent rotating potential of ^{14}Ne as a function of rotational frequency Ω . They are given along the deformation path of the $[1, 1, 1, 1] \otimes [2, 3, 3, 2]$ [panel (a)] and $[1, 1, 1, 1] \otimes [1, 3, 4, 2]$ [panel (b)] occupation blocks (see Sec. 5.2.2 for more details). Long-dashed red, solid black, dot-dashed green, and dotted blue lines indicate $(\pi = +, r = +i)$, $(\pi = +, r = -i)$, $(\pi = -, r = +i)$, and $(\pi = -, r = -i)$ orbitals, respectively. At $\Omega = 0.0$ MeV, the single-particle orbitals are labeled by the asymptotic quantum numbers $K[Nn_z\Lambda]$ (Nilsson quantum numbers) of the dominant component of the wavefunction. Solid circles indicate occupied orbitals in proton unbound and proton bound parts of the configurations. The vertical orange dashed line indicates the frequency (corresponding to spin I_{trans}) at which the configuration becomes proton bound. Intruder orbitals of the M-type before and after band crossing are labelled by I1 and I2 in panel (a). See text for further details.

To build higher angular momentum than the one in the ground state rotational band one should excite the particles from the orbitals with low orbital angular momentum l into the ones with high l values (see Refs. [3, 7]). Thus, the high spin configurations

which are either yrast or located close to the yrast line are expected to be characterized by the occupation of the single-particle orbitals with high values of orbital momentum l (see Ref. [16]). This has interesting consequences for the nuclei near drip lines since the $l = 0$ and $l = 1$ orbitals govern halo properties and particle decay. The centrifugal barrier (see Fig. 1) increases substantially with the increase of l and this leads both to a suppression of halos and particle decays and to a better localization of the wave function of the $l > 1$ orbitals within the nuclear volume [13].

This situation can be illustrated by the analysis of the single-particle routhian diagram shown in Fig. 2 which is obtained in the CRMF calculations. Note that the slope $\partial e_i^\Omega / \partial \Omega$ of the single-particle routhian e_i^Ω shown in this figure indicates its orbital angular momentum l . This is because the value of the single-particle alignment $\langle j_x \rangle = -\partial e_i^\Omega / \partial \Omega$ of the orbital is defined by its orbital angular momentum (see Fig. 1 in Ref. [26]). Note also that high- l orbitals become almost fully aligned with the axis of rotation at relatively low frequencies. By considering the 0 – 4.0 MeV energy range of Fig. 2 one can conclude that on average with increasing rotational frequency the slopes of the single-particle routhians (and, as a result, their angular momentum l) become larger and larger. With increasing rotational frequency the routhians located in the vicinity of the Fermi level dive faster under the effective barrier of Fig. 1 leading to the situation in which particle emission proceeds at the single-particle energies e_i^Ω characterized by a higher value of $E_B - e_i^\Omega$ and the width of the barrier at e_i^Ω .

This analysis suggests that even if the configurations remain quasi-bound the combination of these two factors can lead to an increase of the stability of rotational states with respect of particle emission i.e. to a reduction of decay width with increasing spin. This result is in line with those for rotational 1/2[321] band in ^{39}Mg obtained within particle-plus-core model in Ref. [15] which show drastic decrease of the decay width (from very broad to very narrow resonances) with increasing angular momentum in the band.

To address the second question, let us assume that the routhian diagram presented in Fig. 2(b) is also valid for deformed configurations in the ^{12}O nucleus which has two protons less than ^{14}Ne . Under this assumption, the highest occupied proton single-particle orbitals in ^{12}O are 1/2[101]: the occupation of the single-particle orbitals in this configuration is show by open squares in Fig. 2(b). The rotational band built on this configuration will be weakly bound up to rotational frequency $\Omega \approx 2.0$ MeV and its description in the CRMF framework is the same as for weakly bound configurations in neutron-rich nuclei near the neutron drip line discussed in the CSHF approach in Ref. [13]. However, the excitations [shown by green dashed arrows in Fig. 2(b)] of proton from the 1/2[101]($r = +i$) orbital into either the 1/2[220]($r = -i$) or 3/2[211]($r = -i$) ones lead to the excited configurations in which the proton in the highest occupied orbital is quasi-bound. The rotational bands built on these two configurations are quasi-bound from $\Omega = 0.0$ MeV up to $\Omega \approx 3.0$ MeV. Although this is schematic illustration, fully self-consistent CRMF calculations based on systematic survey of configurations of interest in the nuclei near proton and neutron drip lines confirm this picture and indicate that

particle-bound and quasi-bound rotational bands can coexist in the same nucleus. This typically takes place when the ground state rotational band is weakly bound in the nucleus located near drip line.

To address the third question let us consider the evolution of the single-particle routhians in the $[1, 1, 1, 1] \otimes [2, 3, 3, 2]$ occupation block with increasing rotational frequency shown in Fig. 2(a). The last occupied $3/2[211](r = -i)$ orbital in this configuration is quasi-bound and is characterized by a substantial slope which indicates moderate value of orbital angular momentum l . An unpaired band crossing between this orbital and the I2 one takes place at rotational frequency $\Omega \approx 2.6$ MeV. The I2 orbital is significantly more downsloping with increasing rotational frequency and thus it has substantially larger orbital angular momentum than the $3/2[211](r = -i)$ one. As a consequence, with increasing rotational frequency it becomes bound at $\Omega \approx 3.2$ MeV. Thus, the rotational sequence built on such configuration would exhibit the properties of quasi-bound rotational band at $\Omega < 3.2$ MeV and particle-bound rotational band at higher rotational frequency. Such kind of transition (denoted as a birth of particle-bound rotational bands in Ref. [16]) has been investigated for the first time in neutron-rich nuclei near the neutron drip line in Ref. [16] but as illustrated in the present paper it is active also in very proton-rich nuclei at and beyond spin-zero proton-drip line. Alternative possibility of the transition from particle-bound to quasi-bound rotational band (the death of particle-bound rotational bands in the language of Ref. [16]) with increasing spin also exists but it is less frequent in the calculations. Thus, the present analysis clearly indicates that particle-bound and quasi-bound rotational bands do not exist as strictly separate classes of the bands: the transition between them is possible even within fixed nucleonic configuration.

Note that as collective coordinates the rotational frequency Ω in rotating nuclei and deformation β_i in non-rotating ones can have similar effect on binding of the nucleons. The former case is discussed above. The transformation of the character of single-particle orbitals from unbound/quasi-bound(resonant) to bound and vice versa under the change of deformation are clearly visible in the Nilsson diagrams presented in Refs. [27, 28].

The present analysis clearly illustrates that the building of the angular momentum higher than the one which can be achieved in the ground state rotational band requires particle-hole excitations from the states with low orbital momentum l to the ones with high l values. In the nuclei near drip lines, the latter are typically located at positive energies. Thus, these excitations lead to an increase of centrifugal barrier and, as a consequence, to a significant reduction of the decay width of the rotational states of quasi-bound rotational bands. Moreover, with increasing rotational frequency Coriolis interaction acting on occupied high- j (high- l) orbitals, which are quasi-bound at low frequencies, drives them below zero energy threshold and makes them bound (see also Ref. [16]). Thus, one can conclude that through these two mechanisms the collective rotation can lead to an increase of the stability of nuclear systems. Note that the rotational structures at the spin larger than that generated in the ground state rotational

bands of the very neutron-rich nuclei have been systematically studied only in Ref. [16] in the CRMF framework. In particular, it was shown that the latter mechanism can lead to an extension of nuclear landscape to higher neutron numbers as compared with that obtained at low spin.

4. Fast rotation in proton-rich nuclei: general features

The main focus of the present study is fast rotation in very proton rich nuclei. In such nuclei the situation is drastically different as compared with very neutron rich ones because of the presence of Coulomb barrier [see Fig. 1(b)] which has a substantial value. For example, the Coulomb barrier (at spherical shape) almost linearly increases from 2 to 6 MeV in the $N = Z$ nuclei when Z changes from 10 to 36. In combination with centrifugal barrier [see Fig. 1(b)] it leads to a drastic increase (by many orders of magnitude) of proton emission half-lives as compared with characteristic nuclear timescale of 10^{-22} s [25, 29, 30]. For instance, the present window for the experimental observation of proton emission half-lives in medium mass nuclei ranges from 4.5×10^{-7} s to a few seconds which corresponds to extremely narrow width $\Gamma \approx 10^{-22} - 10^{-15}$ MeV of respective proton resonances [25]. In that respect these quasi-bound proton states are very similar to the bound ones. With decreasing proton number and lowering the Coulomb barrier the proton resonances are expected to become broader but for typical situations of interest they are anticipated to be substantially narrower than the neutron ones discussed earlier. Note that the main focus of this paper is on proton bound parts of rotational bands in which the highest in energy occupied single-particle states are located at negative energies.

5. The details of theoretical calculations

5.1. Theoretical framework

The calculations are performed in the framework of cranked relativistic mean field (CRMF) theory [6, 31]. It represents the realization of covariant density functional theory for rotating nuclei with no pairing correlations in one-dimensional cranking approximation. It has been successfully tested in a systematic way on the properties of different types of rotational bands in the regime of weak pairing such as normal-deformed, superdeformed and smooth terminating bands as well as the bands at the extremes of angular momentum (see Refs. [6, 32] and references therein). We restrict ourselves to reflection symmetric shapes which are dominant deformed shapes in the nuclear chart.

The cranking model is semiclassical in nature (see Sec. 3.4 of Ref. [33]) the microscopic derivation of which is provided in projected approaches (see Sec. 11 in Ref. [33]): the cranking model appear as a limit of these approaches at large deformation. It has a proven track of successful description of rotational structures of different types such as normal- and superdeformed rotational bands, terminating bands, magnetic and

antimagnetic bands across the nuclear chart (see Refs. [1, 2, 3, 6, 7, 8, 9, 35] and references quoted therein). In reality, the absolute majority (more than 90% of the cases) of experimental rotational bands, for which theoretical descriptions exist, have been successfully analyzed in the framework of the cranking model. Note that the rotational structures discussed below have a deformation which is large enough for a cranking model to be valid. Moreover the equivalence of the description of rotating nuclei in the intrinsic (rotating) and laboratory frames was confirmed with good accuracy in Ref. [21] on the example of ^{48}Cr . In addition, earlier investigations of the nuclei in the regions of the nuclear chart located near those studied in the present paper show that cranking model successfully describes experimental data on rotational bands (see Refs. [21, 22, 32, 34]) and provides interesting predictions for the structure of rotational bands in light nuclei (see Refs. [10, 11, 22]). Note that similar to cranking model for rotating nuclei, the transformation to the intrinsic rotating frame is also the most dominant approach in the study of rotating Bose-Einstein condensates (see Ref. [36]) and rotating quark-gluon plasma (see Refs. [37, 38, 39]).

Available studies of high spin properties of rotating $N \approx Z$ nuclei located in the vicinity of the part of nuclear chart under study clearly indicate that static pairing becomes negligible at high spin [22, 32]. This allows safely neglect the pairing correlations in the calculations since the focus of the present study is on the parts of rotational bands which become proton bound at high spin. The spin at which the calculations without pairing become a good approximation to those with pairing depends on the mass region: it is around $I \approx 15\hbar$ in the Kr ($Z \approx 36$) region [32] but decreases with lowering the proton number Z [22] down to approximately $5\hbar$ in the nuclei with $Z \leq 10$. In addition, the pairing is substantially reduced due to blocking in the nucleonic configurations in which the opposite signature orbitals are not pairwise occupied [6, 33]: for such configurations the calculations without pairing reproduce experimental data even at lower spins [32].

The CRMF calculations are carried out with the NL3* covariant energy density functional (CEDF) [40] which is the state-of-the-art functional for nonlinear meson-nucleon coupling model [41]. It is globally tested for ground state observables in even-even nuclei [41]. The CRMF and cranked relativistic Hartree-Bogoliubov (CRHB) calculations with this functional provide a very successful description of different types of rotational bands both at low and high spins [40, 42].

The CRMF equations are solved in the basis of an anisotropic three-dimensional harmonic oscillator in Cartesian coordinates characterized by the deformation parameters β_0 and γ and oscillator frequency $\hbar\omega_0 = 41A^{-1/3}$ MeV (see Refs. [31, 43]). The truncation of the basis is performed in such a way that all states belonging to the major shells up to $N_F = 16$ fermionic shells for the Dirac spinors and up to $N_B = 20$ bosonic shells for the meson fields are taken into account. This truncation scheme provides sufficient numerical accuracy for the physical observables of interest [16]. To verify that the numerical test of the convergence of the total binding energies as a function of the number of fermionic shells N_F has been carried out in a similar fashion

to that done in Ref. [16] (see Fig. 4 in this paper and its discussion). This test covered a number of the configurations of interest in the nuclei ranging from ^{14}Ne up to ^{67}Kr . The results obtained for total binding energies $E(I)$ at a given spin I are very similar to those shown in Fig. 4 (a) of Ref. [16]: the values of $E(I)$ calculated with $N_F = 16$ and $N_F = 20$ differ by no more than several hundred keV. The impact of the increase of N_F is even smaller on the relative energies of different configurations (such as those shown in Fig. 4 below) since the increase of N_F leads to additional binding in all configurations. The density distributions (similar to those shown in Fig. 5 below) obtained with $N_F = 16$ and $N_F = 20$ are also very similar to each other. The evolution of the single-particle energies as a function of N_F for negative energies is very similar to that shown in Fig. 4(b) of Ref. [16]: they stabilize at $N_F \approx 16$. At positive energies, due to the presence of the Coulomb barrier the energies of the single-particle states of interest stabilize at lower N_F (typically at $N_F \approx 16$) as compared with the situation seen for neutron single-particle states near neutron drip line which is illustrated in Fig. 4(b) of Ref. [16]. These results clearly illustrate that the $N_F = 16$, $N_B = 20$ basis provides a sufficient numerical accuracy for systematic studies undertaken in the present paper.

5.2. Nucleonic configurations

5.2.1. Basic features. As mentioned in Sec. 2 the nucleonic configurations participating in collective rotation are built either from only bound single-particle states or from the combination of bound and quasi-bound single-particle states. In the former case one deals with particle-bound rotational bands, while in the latter one with quasi-bound rotational bands. Note that nucleonic configuration ceases to exist when the particle (proton or neutron) is emitted from occupied quasi-bound state(s).

In the present paper as well in Ref. [16] we consider the transition from quasi-bound part of rotational band to particle-bound one: these two parts are built on a fixed nucleonic configuration. Note that due to historical reasons in all theoretical publications the rotation of the nucleus is considered in terms of increasing angular momentum and we follow this tradition in our discussion. In contrast, the situation is opposite in experiment since the feeding of rotational band takes place at high angular momentum and then the angular momentum within the band decreases via the cascade of sequential γ -ray transitions which carry away the angular momentum. Thus, for the type of the bands discussed in the present paper and in Ref. [16] the particle-bound part of rotational band will be populated first in experiment and only then the transition to quasi-bound part of rotational band will take place.

5.2.2. Configuration labelling. In the CRMF calculations, the configurations are specified by the number of particles k_{par}^r (where $k = \pi$ or ν for protons and neutrons, respectively) occupying single-particle orbitals of specific parity par and signature r combinations, namely, by the occupation block $[\nu_+^+, \nu_+^-, \nu_-^+, \nu_-^-] \otimes [\pi_+^+, \pi_+^-, \pi_-^+, \pi_-^-]$. Note that the occupied orbitals are counted from the bottom of nucleonic potential. For

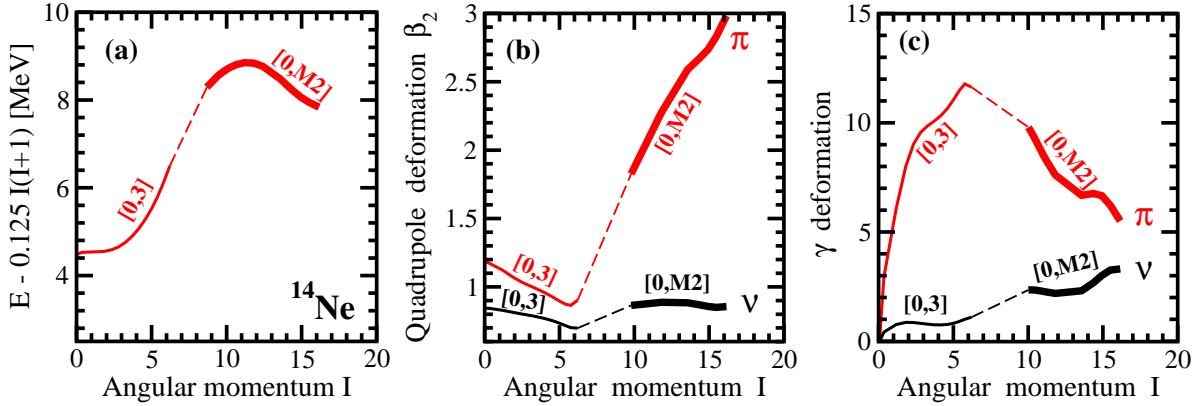


Figure 3. The energies [relative to a smooth liquid drop reference $E_{RLD} = AI(I+1)$] and neutron and proton quadrupole (β_2) and triaxial (γ) deformations of the $[1, 1, 1, 1] \otimes [2, 3, 3, 2]$ occupation block in ^{14}Ne as a function of angular momentum I . The deformation parameters $\beta_2 = \sqrt{\frac{5}{16\pi} \frac{4\pi}{3AR_0^2} \sqrt{Q_{20}^2 + 2Q_{22}^2}}$ and $\gamma = \arctan \sqrt{2} \frac{Q_{22}}{Q_{20}}$ are extracted from respective quadrupole moments $Q_{20} = \int d^3r \rho(\vec{r}) (2z^2 - x^2 - y^2)$ and $Q_{22} = \int d^3r \rho(\vec{r}) (x^2 - y^2)$. Note that $R_0 = 1.2A^{1/3}$.

simplicity we use only the sign for the $r = \pm i$ signature and parity $par = \pm$ in this block. The occupation block $[\nu_+^+, \nu_+^-, \nu_-^+, \nu_-^-] \otimes [\pi_+^+, \pi_+^-, \pi_-^+, \pi_-^-]$ defines the lowest in energy configuration for a given combination of parities and signatures of occupied orbitals. This type of configuration definition is common in density functional theoretical (DFT) calculations without pairing: it is used not only in the CRMF calculations [31, 43], but also in the cranked Skyrme DFT calculations [44, 45].

The rotational and deformation properties of extremely deformed bands strongly depend on intruder content of their configurations. Thus, an alternative way of configuration labeling, frequently used in the literature, is by counting the number of occupied intruder orbitals [43, 46]. This labelling scheme is also used in the present paper since it provides important physical insight on the properties of the bands. Thus, the configurations are labeled by shorthand labels $[n, p_1 p_2]$ where n ($p_1 p_2$) indicates the number of occupied intruder neutron (proton) orbitals. However, the meaning of intruder orbitals depends on the mass region. For example, the configurations $[n, p_1]$ in ^{14}Ne are labeled by the number of occupied $N = 2$ neutron (n) and proton (p_1) intruder orbitals while those in ^{67}Kr by the number of the occupied $N = 4$ neutron (n) intruder orbitals and $N = 4$ (p_1) and $N = 5$ (p_2) proton intruder orbitals. The label p_2 is omitted when $p_2 = 0$.

Note that such labeling is feasible only in the case when more than 50% of intruder orbital wavefunction belongs to a specific N -shell. However, proton intruder orbitals, which are strongly downslowing as a function of rotational frequency in the routhian diagrams at high rotational frequencies (see Fig. 2), are significantly mixed because of the $\Delta N = 2$ interaction. For example, at rotational frequency $\Omega_x = 3.20$ MeV the squared weights a_N^2 of the $N = 2, 4, 6,$ and 8 shells in the structure of the wave function of the intruder I2 orbital of the configuration $[0, M2]$ are 0.09, 0.12, 0.19 and 0.21,

respectively. Note that $\sum_N a_N^2 = 1.0$ (see Sec. D1 in Ref. [47]). As a consequence, there is no single N -shell whose contribution to the structure of the wave function exceed 50%. Such strongly mixed orbitals are called here as M-orbitals and the label "M#" is used in the shorthand $[n, p]$ notation to indicate their presence and their number #. Note that we count total number # of negative and positive parity orbitals when we define the number of the M-orbitals.

The use of such configuration labelling and basic features of calculated configurations are illustrated in Fig. 3 on the example $[1, 1, 1, 1] \otimes [2, 3, 3, 2]$ occupation block in ^{14}Ne . Its calculated $E - E_{RLD}$ curve represents the envelope of two configurations defined in terms of the occupation of intruder orbitals, namely, the $[0, 3]$ and $[0, \text{M}2]$ [see Fig. 3(a)]. The configuration change from $[0, 3]$ to $[0, \text{M}2]$ within this occupation block is due to unpaired band crossing related to the crossing of the single-particle orbitals which takes place at rotational frequency $\Omega \approx 2.6$ MeV (see Fig. 2). It triggers substantial changes in equilibrium deformations and their evolution with angular momentum [see Figs. 3(b) and (c)].

The lines of different styles are used in Fig. 3 and throughout the paper to discriminate between different parts of the $E - E_{RLD}$ curve corresponding to a given occupation block. In this paper, proton unbound and/or quasi-bound parts of the rotational bands [such as configuration $[0, 3]$ in Fig. 3] are shown by thin solid lines while the proton bound ones [such as the configuration $[0, \text{M}2]$ in Fig. 3] by thick solid line. Since the calculations are performed as a function of rotational frequency, the solutions are not available for some spin range in the region of band crossing. Thus, we use dashed thin line to connect the configurations, defined in terms of intruder orbitals, within the envelope of the specific occupation block (see Fig. 3).

6. The birth of proton-bound rotational bands in ^{14}Ne and ^{67}Kr nuclei

To illustrate the basic features of rotation in very proton rich nuclei and their dependence on the mass region we consider the examples of the ^{14}Ne and ^{67}Kr nuclei. ^{14}Ne is an extremely proton rich nucleus with 10 protons and only 4 neutrons and ^{67}Kr has 36 protons and 31 neutrons. In the Ne isotopic chain the last proton bound even-even nucleus is ^{18}Ne in the RHB calculations at spin $I = 0$ which agrees with the fact that experimentally measured ^{16}Ne is located beyond the two-proton drip line [41]. These calculations also predict that the last proton bound Kr isotope is ^{68}Kr . This is in agreement with the observation of two proton radioactivity in ^{67}Kr [48, 49].

The calculated configurations of the ^{14}Ne and ^{67}Kr nuclei are shown in Fig. 4. One can see that absolute majority of the configurations in these nuclei are proton quasi-bound at low spin but with increasing spin and undergoing band crossing these configurations become proton bound. The microscopic origin of this transition is illustrated in Fig. 2 on the example of proton single-particle routhian diagram corresponding to the $[1, 1, 1, 1] \otimes [2, 3, 3, 2]$ occupation block which leads to the $[0, 3]$ and $[0, \text{M}2]$ configurations (in terms of intruder orbitals) at low and high spins [see

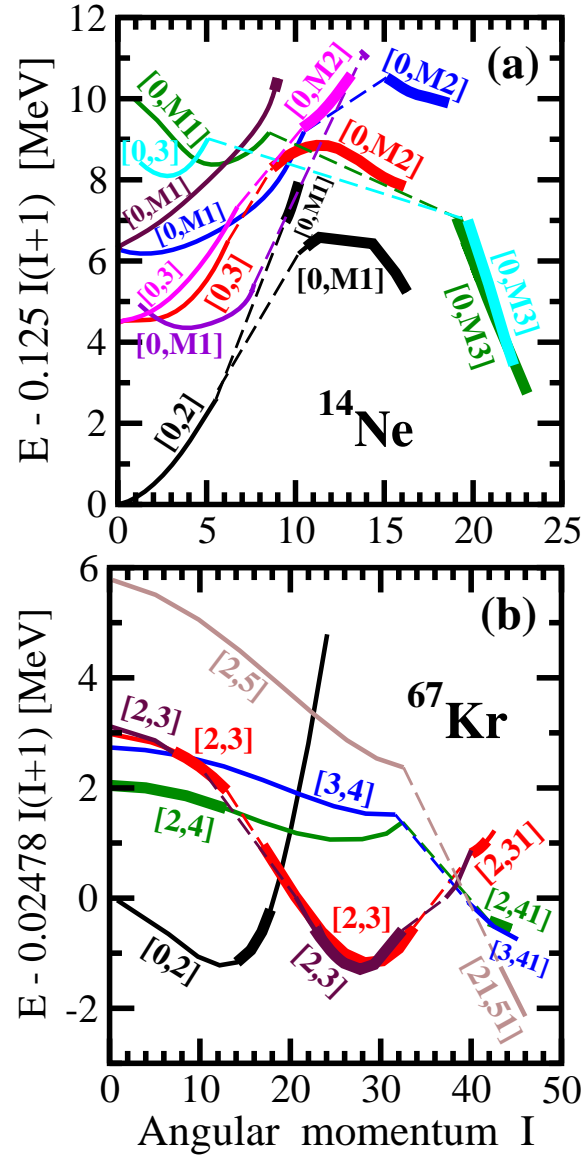


Figure 4. The energies of calculated configurations in ^{14}Ne and ^{67}Kr relative to a smooth liquid drop reference $AI(I+1)$. The numerical values of inertia parameter A are indicated on vertical axis. Additional information on the configurations of these nuclei are displayed in Table 1.

red lines in Fig. 4(a)], respectively. At low and medium rotational frequencies Ω_x , the occupied proton $1/2[220](r = +i)$ and $3/2[211](r = -i)$ orbitals are located at positive energies [see Fig. 2(a)]. Thus, the $[0, 3]$ configuration is proton quasi-bound. However, with increasing rotational frequency intruder orbitals I1 and I2 of negative and positive parities become occupied at $\Omega_x \approx 2.9$ MeV leading to the $[0, M2]$ configuration which becomes proton bound at $\Omega = 3.19$ MeV. This microscopic mechanism of the creation of proton bound rotational bands from proton quasi-bound ones is equivalent to the birth of particle bound rotational bands in very neutron rich nuclei near neutron drip line discussed earlier in Ref. [16]. Note that this mechanism is active in all nuclei studied in

Table 1. The configurations calculated in the ^{14}Ne and ^{67}Kr nuclei. The first column specifies the occupation blocks of the configurations. The second column identifies the configurations in terms of intruder orbitals corresponding to the respective occupation block: the first/second label corresponds to low/high spin configurations. The total parity π_{tot} and signature r_{tot} of the occupation block are listed as (π_{tot}, r_{tot}) in the last column.

occupation block	configurations	(π_{tot}, r_{tot})
1	2	3
^{14}Ne [$N = 4, Z = 10$]		
$[1, 1, 1, 1] \otimes [2, 2, 3, 3]$	$[0,2], [0,M1]$	$(+, +)$
$[1, 1, 1, 1] \otimes [2, 3, 3, 2]$	$[0,3], [0,M2]$	$(-, +)$
$[1, 1, 1, 1] \otimes [1, 3, 4, 2]$	$[0,M1], [0,M3]$	$(+, +)$
$[1, 1, 1, 1] \otimes [2, 2, 4, 2]$	$[0,M1], [0,M2]$	$(+, -)$
$[1, 1, 1, 1] \otimes [2, 2, 2, 4]$	$[0,M1], [0,M1]$	$(+, -)$
$[1, 1, 1, 1] \otimes [1, 2, 4, 3]$	$[0,M1], [0,M2]$	$(-, +)$
$[1, 1, 1, 1] \otimes [1, 4, 3, 2]$	$[0,3], [0,M3]$	$(-, -)$
$[1, 1, 1, 1] \otimes [3, 2, 3, 2]$	$[0,3], [0,M2]$	$(-, -)$
$[1, 1, 1, 1] \otimes [2, 2, 3, 3]$	$[0,2], [0,M1]$	$(+, +)$
^{67}Kr [$N = 31, Z = 36$]		
$[7, 7, 9, 8] \otimes [8, 8, 10, 10]$	$[0,2]$	$(-, +)$
$[8, 8, 8, 7] \otimes [8, 9, 9, 10]$	$[2,3], [2,31]$	$(+, -)$
$[8, 8, 8, 7] \otimes [9, 9, 9, 9]$	$[2,4], [2,41]$	$(-, +)$
$[8, 9, 7, 7] \otimes [9, 9, 9, 9]$	$[3,4], [3,41]$	$(+, -)$
$[8, 8, 7, 8] \otimes [8, 9, 10, 9]$	$[2,3], [2,31]$	$(+, -)$
$[8, 8, 8, 7] \otimes [10, 9, 9, 8]$	$[2,5], [21,51]$	$(+, -)$

Sec. 8 below.

An interesting feature of these rotational structures is the fact that at least 80% of the angular momentum is built in the proton subsystem because of limited angular momentum content in the neutron one. Thus, the neutron subsystem behaves as a spectator in building collective rotation.

By performing the calculations for the ^{14}Ne nucleus with the DD-MEX and NL1 [50] covariant energy density functionals it was verified that the general results obtained in the present paper are not affected by the selection of the functional.

7. Giant proton halo in rotating very proton-rich nuclei

The above discussed features and transition to exceedingly proton rich nuclei lead to significant modifications in density distributions which are especially pronounced in light nuclei. For example, the imbalance between protons and neutrons leads to a substantial proton skin and/or halo already at low spin in all calculated configurations of ^{14}Ne . This is illustrated by the comparison of neutron and proton densities of the $[0, 3]$ configuration

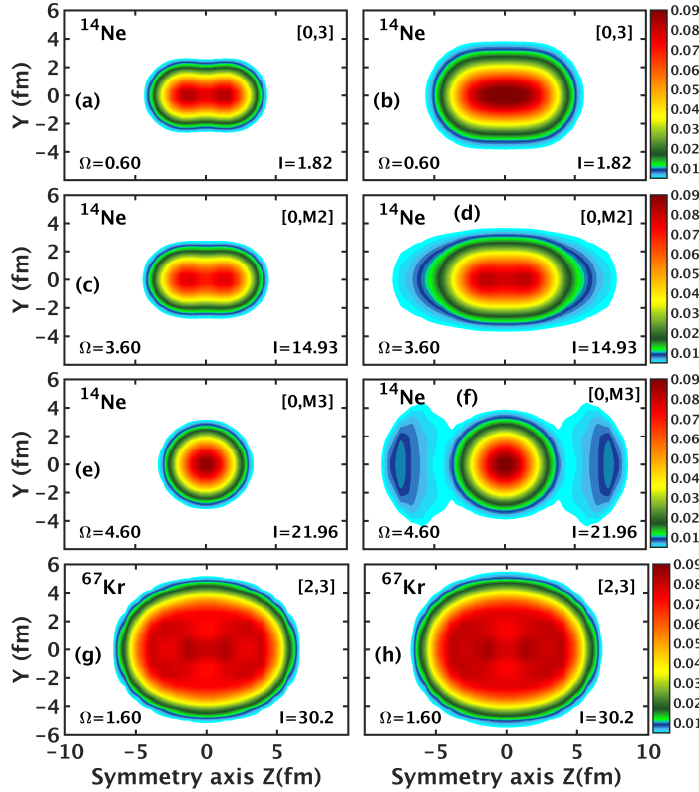


Figure 5. Neutron (left column) and proton (right column) density distributions of the configurations in ^{14}Ne and ^{67}Kr at indicated spins and frequencies. The density colormap starts at $\rho = 0.005 \text{ fm}^{-3}$ and shows the densities in fm^{-3} .

in Figs. 5(a) and (b). Additional proton particle-hole excitations leading to the $[0, M2]$ configuration generate low density giant proton halo which is especially extended in the equatorial region [see Fig. 5(d)]. Note that this particle-hole excitation has only small impact on the neutron densities (compare Figs. 5(a) and (c)) indicating that there is a substantial decoupling of proton and neutron degrees of freedom due to underlying shell structure.

These two subsystems of the $[0, M2]$ configuration have drastically different quadrupole (β_2) and triaxial (γ) deformations which also behave differently as a function of angular momentum [see Fig. 3(b) and (c)]. The β_2 and γ deformations of the neutron subsystem almost do not change with increasing angular momentum. In contrast, the quadrupole deformation β_2 of proton subsystem drastically increases with increasing angular momentum due to the centrifugal stretching of the nucleus [see Fig. 3(b)]. Similar (but significantly less pronounced) processes have been seen before in the calculations of many hyper- and megadeformed rotational bands in the $A \approx 40$ $N \approx Z$ (see Ref. [22]) and $Z = 40-58$ (see Ref. [47]) regions of nuclear chart. The γ -deformation of proton subsystem decreases fast with increasing angular momentum.

Additional particle-hole excitations lead to more exotic nuclear shapes. For example, the excitation indicated by blue arrow in Fig. 2 leads to the occupation block $[1, 1, 1, 1] \otimes [1, 3, 4, 2]$ which corresponds to the envelope of the $[0, 3]$ and $[0, M3]$

configurations shown in cyan in Fig. 4. The densities of low spin [0,3] configuration are similar to those shown in Fig. 5(a) and (b). However, the ones for the high spin [0, M3] configuration are built of near spherical shape for neutron densities [Fig. 5(e)] and cluster-type giant proton halo in proton subsystem [Fig. 5(f)]. The latter consist of high density prolate central cluster and low (with $\rho \approx 0.01 \text{ fm}^3$) density clusters centered at around $z \approx \pm 7 \text{ fm}$.

The kinematic moments of inertia $J^{(1)}$ and transition quadrupole moments Q_t of the bands with giant proton halos are substantially larger than those of the ground state rotational band. For example, in the ^{14}Ne nucleus the kinematic moment of inertia of the ground state band is $J^{(1)} \approx 2.2 \text{ MeV}^{-1}$ at spin $I = 2\hbar$, while that for the [0,M3] configurations shown in Fig. 4(a) is $J^{(1)} \approx 5.3 \text{ MeV}^{-1}$ at $I \approx 20\hbar$. The Q_t values for the ground state and giant proton halo rotational bands are $Q_t \approx 0.55 \text{ eb}$ and $Q_t \approx 1.4 \text{ eb}$, respectively. These large differences in the physical observables could be used for an experimental identification of potential candidates for giant proton halo structures.

Note that the processes of the creation of proton halos are suppressed in higher Z nuclei due to smaller imbalances between protons and neutrons and reduced relative impact of a given single-particle orbital into the buildup of the total densities. This is illustrated by the comparison of the proton and neutron density distributions in the [2, 3] configuration of ^{67}Kr [Figs. 5(g) and (h)].

The physical mechanism of the creation of giant proton halos in rotating nuclei is completely different as compared with that predicted for non-rotating proton rich nuclei. In the latter ones, it is based on the occupation of loosely bound s and p orbitals [51, 52, 53]. In contrast, it is due to either a significant excess of protons over neutrons [compare Figs. 5(a) and (b)] or the occupation of intruder strongly-mixed M-orbitals [Figs. 5(d) and (f)]. The wave functions of the later ones contain significant admixtures from the high N shells (see example in Sec. 5.2.2). Note also that in many cases these orbitals are deeply bound: the Fermi levels, corresponding to the energy of the last occupied orbital, of the configurations of interest is located in the range between -4 to -2.5 MeV at the highest calculated rotational frequencies (see, for example, Fig. 2). The nodal structure of these intruder orbitals (see discussion in Ref. [12]) plays an important role in the creation of the halo and cluster type structures of rotating nuclei under study.

8. Rotation induced extension of the nuclear landscape

An impact of rotation on the properties of very proton rich nuclei similar to that discussed in Sec. 6 has been found for even Z isotopic chains with $4 \leq Z \leq 36$. Here, we focus on rotation induced extension of the nuclear landscape presented in Fig. 6. Colored squares or circles in this figure are used for the nuclei which are proton unbound or quasi-bound at no rotation, but some configurations of which become proton bound when the nucleus rotates.

The lowest spin ranges (in step of $5\hbar$) at which proton bound configurations appear

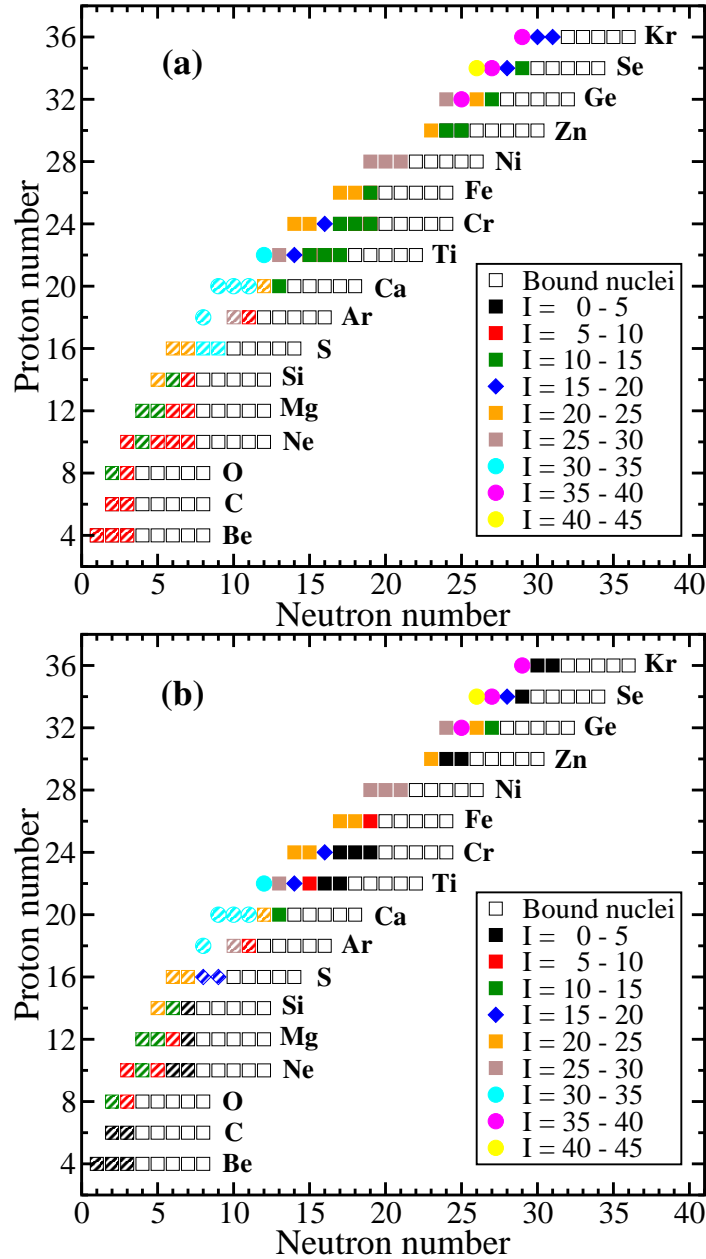


Figure 6. Rotation induced extension of the nuclear landscape. Open squares show the nuclei which are proton bound at no rotation in the RHB calculations of Ref. [41]: these predictions are compared with experimental data in Sec.VII of Ref. [41]. Colored squares, diamonds and circles show the lowest spin range (in step of $5\hbar$) at which proton bound configurations appear in the calculations. In panel (a) they are only shown above the lowest spins I_{unpair} above which the disappearance of static pairing correlations along the yrast line is expected while in panel (b) they are displayed at spin values at which the configurations become proton bound in the CRMF calculations (see text for details). Dashed filling pattern is used to indicate the nuclei in which at least one nucleonic configuration with rotation induced giant proton halo of the types shown in Figs. 5(d) and (e) appear in the calculations.

in the calculations are defined in the following way. In Fig. 6(a), they are shown above the lowest spins I_{unpair} for which the disappearance of static pairing correlations is expected. The results of the CRHB calculations and the comparison with the ones of the CRMF calculations indicates that static pairing disappears at $I_{unpair} \approx 5\hbar$, $I_{unpair} \approx 10\hbar$ and $I_{unpair} \approx 15\hbar$ in the Ne, Ca and Kr nuclei, respectively (see Refs. [22, 32]). Thus, I_{unpair} is set at $5\hbar$ for the nuclei with $Z \leq 10$ and then gradually increases from $5\hbar$ up to $10\hbar$ for the nuclei with $12 \leq Z \leq 20$ and from $10\hbar$ up to $15\hbar$ for the nuclei with $22 \leq Z \leq 36$. Note that above these spins we consider not only yrast but also excited configurations which are located not significantly higher than 2 MeV above the yrast line. The configurations located at higher excitation energies are excluded from the analysis since rotational damping may lead to a disappearance of discrete rotational bands [54].

The existing experience with CRHB and CRMF calculations shows that static pairing correlations could disappear due to the combination of blocking and Coriolis anti-pairing effects at spins below I_{unpair} when the configurations are based on particle-hole excitations. Thus, in Fig. 6(b) we also show the lowest spins I_{lowest} ($I_{lowest} < I_{unpair}$) at which such configurations become proton bound in the calculations without pairing. This leads to lowering of the spins as compared with those given in Fig. 6(a) in some nuclei (such as $^{16,17}\text{Ne}$) located close to the proton drip line. The CRHB calculations with pairing are needed to either confirm or reject this lowering of the spins but they go beyond the scope of the present paper. Note that for $I < I_{unpair}$ we consider only the yrast configurations.

Fig. 6 shows that in many nuclei located beyond $I = 0$ proton drip line the transition to proton bound configurations takes place at relatively modest spin values. However, in a given isotopic chain such transition occurs at higher spin values with increasing proton excess. In addition, the calculations suggest that the formation of rotation induced giant proton halos is feasible only in the $Z \leq 20$ nuclei.

It is necessary to recognize that the rotational excitations in such proton-rich nuclei (with considerable excess of the protons over neutrons in light nuclei) have not been experimentally studied so far. However, recent experimental studies of the ^9N nucleus indicate the existence of the quasi-bound (resonance) states (see Refs. [55, 56]) on base of which the rotational excitations can be built. Note that this is extremely proton-rich nucleus which consists of seven protons and only two neutrons: the proton/neutron ratio Z/N for this nucleus is 3.5 which is substantially larger than the $Z/N = 2.5$ value for the ^{14}Ne nucleus discussed in Sec. 6. This suggests that in principle such experimental studies may be feasible in the future.

9. Conclusions

The detailed investigation of fast rotation in the nuclei located in the vicinity of the drip lines defined at no rotation and beyond has been carried out in the cranked relativistic mean field approach. The primary attention has been paid to very proton rich rotating

nuclei. The main results of this study can be summarized as follows.

- The analysis of existing theoretical studies of the rotation in the nuclei near and beyond drip lines indicates that collective rotation can lead to an increase of the stability of nuclear systems via two mechanisms. In the first one, the particle-hole excitations from the states with low orbital momentum l to the ones with high l values lead to an increase of centrifugal barrier of quasi-bound single-particle states occupied in the nucleonic configuration. This leads to a significant reduction of the decay width of the rotational states of quasi-bound rotational bands. In the second one, with increasing rotational frequency Coriolis interaction acting on occupied high- j (high- l) orbitals, which are quasi-bound at low frequencies, drives them below zero energy threshold and makes them bound.
- For the first time we show that rotational bands which are proton quasi-bound at zero or low spins can be transformed into proton bound ones by collective rotation of nuclear systems. Strong Coriolis interaction acting on high- j or strongly mixed M orbitals provides a microscopic mechanism for this transformation by driving the highest in energy occupied single-particle states of nucleonic configurations into negative energy domain. These rotational bands, which in the language of Ref. [16] undergo the birth of particle bound parts at high spin, are transitional in nature between classical particle-bound rotational bands which at present are almost exclusively observed in experiment [2, 5, 7, 54] and very rare examples of quasi-bound rotational bands [14, 15].
- The calculations indicate the presence of rotation induced giant proton halo in the nucleonic configurations which are typically proton bound at high spin. Few of these configurations reveal underlying clustering structures. Their formation is triggered by the occupation of strongly mixed M intruder orbitals. Thus, the physical mechanism of the creation of giant proton halos in rotating nuclei is completely different as compared with non-rotating nuclei in which the formation of proton halo proceeds via the occupation of loosely bound s and p orbitals [51, 52, 53].
- The birth of proton bound rotational bands leads to a substantial extension of nuclear landscape towards more proton rich nuclei as compared with the one defined in non-rotating nuclei. This is similar to the extension of nuclear landscape towards more proton rich nuclei on transition from ellipsoidal to toroidal shapes in hyperheavy nuclei [57]. In both cases, the change of collective coordinates (deformation in hyperheavy nuclei and combination of deformation and rotational frequency in rotating nuclei) triggers the modification of underlying single-particle structure in such a way that occupied states become proton bound above some values of these coordinates. Note that in a given isotopic chain the transition due to collective rotation to proton bound configurations occurs at higher spin values with increasing proton excess.

This material is based upon work supported by the U.S. Department of Energy,

Office of Science, Office of Nuclear Physics under Award No. DE-SC0013037. Useful discussions with Profs. A. Volya and D. Vretenar are greatly appreciated.

- [1] Z. Szymański, *Fast nuclear rotation* (Clarendon Press, Oxford, 1983).
- [2] M.J.A. de Voigt, J. Dudek, Z. Szymański, High-spin phenomena in atomic nuclei, *Rev. Mod. Phys.* **55**, 949 (1983).
- [3] S. G. Nilsson and I. Ragnarsson, *Shapes and shells in nuclear structure*, (Cambridge University Press, 1995).
- [4] P.J. Twin *et al*, Observation of a Discrete-Line Superdeformed Band up to $60\hbar$ in ^{152}Dy , *Phys. Rev. Lett.* **57**, 811 (1986).
- [5] C. Baktash, B. Haas, W. Nazarewicz, Identical bands in deformed and superdeformed nuclei. *Annu. Rev. Nucl. Part. Sci.* **45**, 485 (1995).
- [6] D. Vretenar, A.V. Afanasjev, G.A. Lalazissis and P. Ring, Relativistic Hartree-Bogoliubov theory: Static and dynamic aspects of exotic nuclear structure, *Phys. Rep.* **409**, 101 (2005).
- [7] A.V. Afanasjev, D.B. Fossan, G.J. Lane, I. Ragnarsson, Termination of rotational bands: Disappearance of quantum many-body collectivity. *Phys. Rep.* **322**, 1 (1999).
- [8] S. Frauendorf, Spontaneous symmetry breaking in rotating nuclei, *Rev. Mod. Phys.* **73**, 463 (2001).
- [9] J.Meng, J.Peng, S.-Q.Zhang and P.-W.Zhao, Progress on tilted axis cranking covariant density functional theory for nuclear magnetic and antimagnetic rotation, *Front. Phys.* **8**, 55 (2013).
- [10] T. Ichikawa, J.A. Maruhn, N. Itagaki, and S. Ohkubo, Linear Chain Structure of Four- α Clusters in ^{16}O , *Phys. Rev. Lett.* **107**, 112501 (2011).
- [11] P.W. Zhao, N. Itagaki, and J. Meng, Rod-shaped Nuclei at Extreme Spin and Isospin, *Phys. Rev. Lett.* **115**, 022501 (2015).
- [12] A.V. Afanasjev and H. Abusara, From cluster structures to nuclear molecules: The role of nodal structure of the single-particle wave functions, *Phys. Rev. C* **97**, 024329 (2018).
- [13] W. Nazarewicz, J. Dobaczewski, M. Matev, S. Mizutori, and W. Satula, Rotational properties of neutron drip line nuclei, *Acta Phys. Pol. B* **32**, 2349 (2001).
- [14] K. Fosse, W. Nazarewicz, Y. Jaganathen, N. Michel, M. Płoszajczak, Nuclear rotation in the continuum, *Phys. Rev. C* **93**, 011305 (2016).
- [15] K. Fosse, W. Nazarewicz, Y. Jaganathen, N. Michel, M. Płoszajczak, Single-particle and collective motion in unbound deformed ^{39}Mg , *Phys. Rev. C* **94**, 054302 (2016).
- [16] A.V. Afanasjev, N. Itagaki, D. Ray, Rotational excitations in near neutron-drip line nuclei: The birth and death of particle-bound rotational bands and the extension of nuclear landscape beyond spin zero neutron drip line, *Phys. Lett. B* **794**, 7 (2019).
- [17] D. Rudolph *et al*, Prompt proton decay scheme of ^{59}Cu , *Phys. Rev. Lett.* **89**, 022501 (2002).
- [18] D. Seweryniak *et al*, Rotational bands in the proton emitter ^{141}Ho , *Phys. Rev. Lett.* **86**, 1458 (2001).
- [19] M. Thoennessen, Reaching the limits of nuclear stability. *Rep. Prog. Phys.* **67**, 1187 (2004).
- [20] D.S. Delion and S. Ghinescu, Systematics of neutron emission, nuclear theory archive arXiv:2311.08180v1 (2023).
- [21] E. Caurier, J.L. Egido, G. Martínez-Pinedo, A. Poves, J. Retamosa, L.M.Robledo and A.P. Zuker, Intrinsic vs laboratory frame description of the deformed nucleus ^{48}Cr , *Phys. Rev. Lett.* **75**, 2466 (1995).
- [22] D. Ray and A.V. Afanasjev, From superdeformation to extreme deformation and clusterization in the $N \approx Z$ nuclei of the $A \approx 40$ mass region, *Phys. Rev. C* **94**, 014310 (2016).
- [23] J.J. Sakurai, *Modern Quantum Mechanics* (Addison-Wesley, 1994).
- [24] Y.D. Chong, *Quantum Mechanics III* (LibreTexts, 2023).
- [25] S. Åberg, P.B. Semmes and W. Nazarewicz, Spherical proton emitters, *Phys. Rev. C* **56**, 1762 (1997).

- [26] S. Zhu *et al*, Investigation of antimagnetic rotation in ^{100}Pd , Phys. Rev. C **64**, 041302(R) (2001).
- [27] I. Hamamoto, Nilsson diagrams for light neutron-rich nuclei with weakly-bound neutrons, Phys. Rev. C **76**, 054319 (2007).
- [28] I. Hamamoto, Shape and shell structure of lighter ($N \leq 90$) neutron-rich nuclei based on phenomenological Woods-Saxon potential, Phys. Rev. C **99**, 024319 (2019).
- [29] P.J. Woods and C.N. Davids, Nuclei beyond the proton drip-line, Ann. Rev. Nucl. Part. Sc. **47**(1), 541 (1997).
- [30] D.S. Delion, R.J. Liotta and R. Wyss, Systematics of proton emission, Phys. Rev. Lett. **96**, 072501 (2006).
- [31] W. Koepf and P. Ring, A relativistic description of rotating nuclei: the yrast line of ^{20}Ne , Nucl. Phys. A **493**, 61 (1989).
- [32] A.V. Afanasjev and S. Frauendorf, Description of rotating $N = Z$ nuclei in terms of isovector pairing, Phys. Rev. C **71**, 064318 (2005).
- [33] P. Ring and P. Schuck, *The Nuclear Many-Body Problem* (Springer-Verlag, Berlin) (1980).
- [34] A.V. Afanasjev, I. Ragnarsson, P. Ring, Comparative study of superdeformed and highly deformed bands in the $a \sim 60$ mass region. Phys. Rev. C **59**, 3166 (1999)
- [35] R. Bengtsson, S. Frauendorf, An interpretation of backbending in terms of the crossing of the ground state band with an aligned two-quasiparticle band. Nucl. Phys. A **314**(1), 27 – 36 (1979)
- [36] A.L. Fetter, Rotating trapped bose-einstein condensates. Rev. Mod. Phys. **81**, 647 (2009).
- [37] Y. Jiang, Z.-W. Lin and J. Liao, Rotating quark-gluon plasma in relativistic heavy ion collisions. Phys. Rev. C **94**, 044910 (2016).
- [38] M.N. Chernodub, S. Gongyo, Interacting fermions in rotation: chiral symmetry restoration, moment of inertia and thermodynamics. Jour. High En. Phys. **1**, 136 (2017).
- [39] S. Ebihara, K. Fukushima, K. Mameda, Boundary effects and gapped dispersion in rotating fermionic matter. Phys. Lett. B **764**, 94 (2017).
- [40] G.A. Lalazissis, S. Karatzikos, R. Fossion, D.P. Arteaga, A.V. Afanasjev, P. Ring, The effective force NL3 revisited, Phys. Lett. **B671**, 36 (2009).
- [41] S.E. Agbemava, A.V. Afanasjev, D. Ray and P. Ring, Global performance of covariant energy density functionals: Ground state observables of even-even nuclei and the estimate of theoretical uncertainties, Phys. Rev. C **89**, 054320 (2014).
- [42] A.V. Afanasjev and O. Abdurazakov, Pairing and rotational properties of actinides and superheavy nuclei in covariant density functional theory, Phys. Rev. C **88**, 014320 (2013).
- [43] A.V. Afanasjev, J. König and P. Ring, Superdeformed rotational bands in the $A \sim 140 - 150$ mass region: A cranked relativistic mean field description, Nucl. Phys. A **608**, 107 (1996).
- [44] Y. Shi, J. Dobaczewski, S. Frauendorf, W. Nazarewicz, J.C. Pei, F.R. Xu, and N. Nikolov, Self-consistent tilted-axis-cranking study of triaxial strongly deformed bands in ^{158}Er at ultrahigh spin, Phys. Rev. Lett. **108**, 092501 (2012).
- [45] K. Yoshida, Super- and hyperdeformation in ^{60}Zn , ^{62}Zn , and ^{64}Ge at high spins, Phys. Rev. C **105**, 024318 (2022).
- [46] W. Nazarewicz, R. Wyss and A. Johnson, Structure of superdeformed bands in the $A \approx 150$ mass region, Nucl. Phys. A **503**, 285 (1989).
- [47] A.V. Afanasjev and H. Abusara, Hyperdeformation in the cranked relativistic mean field theory: The $Z = 40 - 58$ region of the nuclear chart, Phys. Rev. C **78**, 014315 (2008).
- [48] T. Goigoux *et al*, Two-proton radioactivity of ^{67}Kr , Phys. Rev. Lett. **117**, 162501 (2016).
- [49] S.M. Wang and W. Nazarewicz, Puzzling two-proton decay of ^{67}Kr , Phys. Rev. Lett. **120**, 212502 (2018).
- [50] P.G. Reinhard, M. Rufa, J. Maruhn, W. Greiner and J. Friedrich, Nuclear ground state properties in a relativistic meson field model, Z. Phys. A **323**, 13 (1986).
- [51] B. Brown and P. Hansen, Proton halos in the $1s0d$ shell, Phys. Lett. B **381**(4), 391 (1996).
- [52] X.Z. Cai *at al*, Existence of a proton halo in ^{23}Al and its significance, Phys. Rev. C **65**, 024610

(2002).

- [53] A.S. Jensen, K. Riisager, D.V. Fedorov and E. Garrido, Structure and reactions of quantum halos, *Rev. Mod. Phys.* **76**, 215 (2004).
- [54] T. Døssing, B. Herskind, S. Leoni, A. Bracco, R. Broglia, M. Matsuo and E. Vigezzi, Fluctuation analysis of rotational spectra, *Phys. Rep.* **268**(1), 1 (1996).
- [55] R.J. Charity and L.G. Sobotka, Invariant-mass spectroscopy in projectile fragmentation reactions, *Phys. Rev. C* **108**, 044318 (2023).
- [56] R.J. Charity *et al*, Strong evidence for ${}^9\text{N}$ and the limits of existence of atomic nuclei, *Phys. Rev. Lett.* **131**, 172501 (2023).
- [57] S.E. Agbemava and A.V. Afanasjev, Hyperheavy spherical and toroidal nuclei: The role of shell structure, *Phys. Rev. C* **103**, 034323 (2021).